ASTRONOMY & ASTROPHYSICS
SUPPLEMENT SERIES

Astron. Astrophys. Suppl. Ser. **129,** 517-540 (1998)

BVRI imaging of M51-type interacting galaxy pairs

I. Data reductions

E. Laurikainen[1,2], **H. Salo**[1,2], **and A. Aparicio**[3]
[1]Division of Astronomy, University of Oulu, PL 333 90571 Oulu, Finland
[2]Instituto de Astronomia, UNAM, Apartado Postal 70-264, Mexico
[3]Instituto de Astrofísica de Canarias, Vía Láctea, E-38200 La Laguna Tenerife, Spain

Received January 31; accepted September 18, 1997

Abstract. Deep broad-band *BVRI* photometry of a sample of 22 closely interacting isolated galaxy pairs is presented. The sample consists of pairs with a large variety of orbital geometries, but most of them are M51-type pairs: a small companion in the vicinity of a prominent two-armed spiral. This subsample will be later modelled in detail with N-body simulations. Nine of the thirteen M51-type pairs show enhanced star formation in the central regions of the companions, detected in $B-V$ or $R-I$ color maps, and only one pair in the nucleus of the main galaxy. This is expected if there is mass transfer from the main galaxy to the companion. Some pairs with larger separation, and with more massive companions show global instabilities manifesting as strong color gradients at least in one of the members.

Key words: galaxies: photometry — galaxies: interactions

1. Introduction

Evidence for enhanced star formation in interacting galaxies has been demonstrated by many research groups focusing on different observational techniques. However, when unbiased samples of interacting- and non-interacting galaxies are compared only, a moderate excess of star formation activity in the very centers of interacting galaxies is found (Bergvall et al. 1997). Telles & Terlevich (1995) have also argued that even most of the HII galaxies, considered as the best candidates for tidally induced starbursts, are hardly triggered by interactions. Indeed, it seems that special galactic disk and perturbation characteristics are needed for enhanced star formation to be induced by galaxy encounters.

Send offprint requests to: E. Laurikainen

Detailed N-body modelling of galaxy pairs gives valuable information of their probable orbital characteristics. For example, our simulation models for Arp 86 (NGC 7753/7752) (Salo & Laurikainen, 1993) and M51 (NGC 5194/5195) (Salo & Laurikainen 1997a) suggest that significant mass transfer to the companion can take place, but only in favorable orbital conditions. The mass flow occurs episodically after the crossing of the main galaxy disk, and may subsequently induce a nuclear starburst in the companion if enough mass is accreted. In the case of Arp 86 the low orbital inclination favours mass accretion, whereas the companion of M51, with almost perpendicular orbit, is expected to be inactive. This scenario is consistent with Hα observations showing a recent starburst in NGC 7752, but not in NGC 5195. Our models for both systems predict bound current orbits and several orbital revolutions inside the halo of the main galaxy before the final merger. We propose that most M51-type pairs represent similar gravitationally bound systems, implying that their star formation properties and spiral patterns are continuously evolving during the course of the orbital evolution. In M51 the models suggest that the long term perturbation from the bound orbit may have induced even the tightly wound innermost spiral arms (Salo & Laurikainen 1997b) observed in near-IR (Zaritsky et al. 1993).

In order to study other similar M51-type pairs, and for comparison with somewhat wider pairs, we have obtained deep *BVRI* images for a sample of galaxy pairs. They were chosen from the "Arp's Atlas of Peculiar Galaxies" (1966) and from the "Catalog of Isolated Pairs of Galaxies in the Northern Hemisphere" by Karachentsev (1972). Deep images enable studies of morphology and stellar distributions both in the inner and outer regions of the galaxies as well as distribution of intermediate age stars. Optical images are especially valuable for detecting the outermost morphology traced by luminous stars. In this paper (Paper I) we present the data reductions and display R, $B-V$ and $R-I$ images. The data analysis is postponed to Paper II

Table 1. The sample

Galaxy	RA (1950) [h m s]	DEC (1950) [° ′ ″]	cz [km s^{-1}]	$T_{\rm m}$[2]	Other name
Arp 70	01:20:41	30:31:25	10494[1]	.S?....	PGC 5085
Arp 74	02:05:17	41:14:33	5543[1]	.SXT5..	PGC 8161
Kar 64 A	02:18:24	39:08:51	7465	.SAS3P.	PGC 8961, Arp 273
Kar 64 B	02:18:27	39:07:43	7335	.SBS1P.	PGC 8970
Kar 125 A	07:06:14	20:40:58	5227[1]	.P.....	PGC 20259, NGC 2341
Kar 125 B	07:06:21	20:43:03	5276[1]	.S...P.	PGC 20265, NGC 2342
Arp 82	08:08:13	25:21:19	4079	.SAR5P.	PGC 22957, NGC 2535
	08:08:16	25:19:46	4142	.SBT5P.	PGC 22958, NGC 2536
Kar 168 A	08:39:53	14:27:58	1988	.S..1..	PGC 24464, Arp 89, NGC 2648
Kar 168 B	08:40:00	14:27	2166		PGC 24469
Kar 179 A	08:53:06	52:17:51	4098	.S?....	PGC 25130
Kar 179 B	08:53:22	52:15:33	3778	.SB.2*.	PGC 25142, NGC 2692
Kar 203 A	09:23:30	68:37:43	3698	.SBS8P.	Arp 300a, Mrk 111,PGC 26849
Kar 203 B	09:23:43	68:38:21	3874	.SXS5.	Arp 300b,PGC 26864
Kar 296 A	11:37:33	15:36:17	3299[1]	.SXT3*P	PGC 36197,Arp 83a, NGC 3800
Kar 296 B	11:37:37	15:37:11	3312[1]	.SBS3*P	PGC 36193,Arp 83b, NGC 3799
Arp 87	11:38:08	22:42:18	7050	.SXT5*P	PGC 36227, NGC 3808
	11:38:08	22:43:22	7189	.I.O.SP	PGC 36228, NGC 3808A
Kar 302 A	11:46:01	48:59:20	944	.SXT5*.	PGC 36875, NGC 3893
Kar 302 B	11:46:19	48:57:10	869	.SB.O*P	PGC 36897, NGC 3896
Kar 331 A	12:18:55	06:55:53	4227	.L.....	NGC 4296,PGC 39943
Kar 331 B	12:18:54	06:56	4046	SO	
Arp 183	13:32:38	31:39:00	4962[1]	.S..3..	PGC 47867
Arp 36	13:31:57	31:40:53	5017[1]	.SB?...	PGC 47808
Kar 404 A	13:56:25	37:41:51	3427	.SBS3P.	PGC 49739, NGC 5394
Kar 404 B	13:56:30	37:40:05	3505	.SAS3P.	PGC 49747, NGC 5395
NGC 5905	15:14:03	55:42:06	3390[1]	.SBR3..	PGC 54445
NGC 5908	15:15:23	55:35:37	3306[1]	.SAS3*/	PGC 54522
Kar 471 A	15:42:36	41:15:00	9480	.S.....	PGC 55913,Mrk 489,NGC 5992
Kar 471 B	15:42:43	41:16:33	9565	.SBR3*.	PGC 55918, NGC 5993
Arp 218	15:51:18	18:45		.SXS4..	PGC 56314
Kar 523 A	17:44:18	35:35	7081		
Kar 523 B	17:44:30	35:35:20	6734	.SB?...	PGC 60829, NGC 6447
Kar 538 A	19:11:53	73:19:30	7510	.SB?...	PGC 62864, NGC 6786
Kar 538 B	19:12:00	73:19	7555	.S?....	PGC 62867
Arp 298	23:00:44	08:36:19	4846	.PSXT1.	PGC 70348, NGC 7469
	23:00:47	08:37:26	4894	.SAR6P	PGC 70350
Arp 86	23:44:33	29:12:22	5163[1]	.SXT4..	PGC 72387,NGC7753
	23:44:27	29:10:52	5072[1]	.I.O*.	PGC 72382,NGC7752, Mrk1134

[1] The radial velocities are from optical measurements, but while marked with superscript they are from 21 cm line measurements.

[2] $T_{\rm m}$ is mean revised morphological type in the RC2 system.

Table 2. The campaigns

Date	Telescope	Pix. size/chip size	seeing	Comment
1990 Jan. 1-5	NOT, 2.5 m	$0.''20/512 * 512$	0.9-1.4	photometric
1990 Feb. 24-27	NOT, 2.5 m	$0.''20/512 * 512$	0.7-2.4	photometric
1991 Jan. 7	JKT, 1.0 m	$0.''30/385 * 585$		partly photom.
1991 July 16-18	NOT, 2.5 m	$0.''20/512 * 512$	0.6-1.0	non-photom.
1991 Aug. 31, Sep 5	Calar Alto, 1.5 m	$0.''32/1024 * 1024$	1.4-2.2	photometric
1992 Feb. 5-12	Calar Alto, 1.5 m	$0.''32/1024 * 1024$	1.1-1.7	partly photom.
1993 Apr. 13-14	NOT, 2.5 m	$0.''20/512 * 512$	0.6-1.3	partly photom.
1993 Nov. 18-20	NOT, 2.5 m	$0.''14/1024 * 1024$	1.0-4.0	non-photom.
1995 Jan. 31	SPM, 2.1 m	$0.''30/1024 * 1024$		photometric

(Laurikainen & Salo, in preparation). A complete observational analysis including HI Fabry-Perot interferometric observations, low- and high resolution IR-images, as well as N-body models for the most interesting M51-type pairs, will be presented later.

2. Sample selection

The sample consists of 22 isolated pairs with a large variety of orbital geometries. The selected pairs show tidal tails and bridges and at least one of the two galaxies is a spiral. We also required that the spiral structure must be well defined. Consequently, merger candidates were excluded (our code is not suitable for studying merging galaxies). The interactions are close, the projected galaxy separations being less than 2 main galaxy diameters (for NGC 5905/5908 the separation is about 3-4 galaxy diameters), and their radial velocity differences are less than 200 km s^{-1}. The sample includes five primary galaxies and six companions with a bar and one with a Seyfert 1 nucleus. Figure 1 displays the digitized Palomar Sky Survey images for the sample pairs converted to common linear kpc scale. On this plot we can see the mutual separations of the pair members as well as appreciate the great variety in the absolute sizes of the sample galaxies.

The sample can be roughly divided to two subgroups: "M51-type" pairs and "others". In M51-type pairs (see Fig. 1a) the main galaxy has deeply penetrating two-armed spirals (so called Grand-Design arms) and a small companion in its vicinity. These systems are likely candidates for mass exchange. The projected position of the companion often falls at the end of a tidal arm, but not necessarily: we are also interested in other cases since even if there has been material flows along the tidal arms the relative position of the companion may have already changed during the encounter. Similarly, projected superposition does not necessarily imply true material connection. Indeed, reliable assertions concerning the role of mass flows become possible only after constructing models for the likely orbital geometry of each individual pair. As the mass of the companion in M51-type pairs is small, and the companion most probably resides inside the halo of the main galaxy, these systems are good candidates for gravitationally bound systems experiencing several orbital revolutions before the final merger due to dynamical friction. Thirteen of the sample pairs belong to this group, and they will be in the focus of our future investigations.

The remaining 9 pairs (see Fig. 1b) are examples of more distant interactions. In most cases the spiral arms are not as regular as the arms of M51-type galaxies and the companions are more massive. In these systems no mass transfer between the encountering galaxies is expected.

3. Reduction

Deep broad-band optical images were obtained during 1990-1995. $BVRI$ images of Arp 86 have been published earlier (Laurikainen et al. 1993) and are not reported here. Table 1 lists the sample galaxies: if not otherwise mentioned the data is from the "Third Reference Catalogue of Bright Galaxies" (de Vaucouleurs et al. 1991). Other name is given if the galaxy has PGC, NGC, Arp or Mrk designation. $T_{\rm m}$ denotes the mean revised morphological type in the RC3 system, and cz is the heliocentric radial velocity of the galaxy. The observations were carried out with the 1.5 m telescope of the Observatorio Astronomico National in Calar Alto, the 1 m Jacobus Kapteyn Telescope (JKT) and the 2.5 m Nordic Optical Telescope (NOT) in La Palma, and the 2.1 m telescope in San Pedro Martir (SPM) in Baja California. In most cases the filters were in the Cousin's $BVRI$ photometric system, but at NOT Thuan-Gunn $r_{\rm TG}$ and $i_{\rm TG}$ filters, attached to the Stockholm CCD, were used. We also measured some galaxies without any filter, designated as *bl* in Table 3. The log of observations is given in Table 2, showing the pixel sizes, CCD-fields and weather conditions for the different observing runs. In Table 3 we show the filters, rebinning factors used while constructing the color maps and the telescopes used. The integration times

were 40−120 minutes in B band, 20−90 minutes in V and 20−60 minutes in R and I bands.

The Stockholm CCD at NOT (512 × 512) was non-linear prior to the year 1993, deviating from linearity about 10%. This non-linearity was corrected by applying an ADU-level dependent correction to each pixel assuming that the non-linearity occurs after the bias addition. The empirical relations by Kjeldsen (1990, private communication) were applied.

Table 3. Observations

Galaxy	Filters	Rebin	Telescope
Arp 70	$BVRIbl$	1	NOT, Nov. 1993
Arp 74	$BVRIbl$	1	NOT, Nov. 1993
Kar 64 AB	VRI	3	Calar Alto, Feb. 1992
Kar 64 A,B	B	1	NOT, Nov. 1993
Kar 125 AB	$BVRI$	4	NOT, July 1991
Arp 82 AB	$BVRIbl$	1	SPM, Jan. 1995
Kar 168 AB	$BVRI$	2	Calar Alto, Feb. 1992
Kar 179 A	$BVRI$	1	NOT, Nov. 1993
Kar 179 B	$BVRIbl$	1	
Kar 203 A	$BVr_{\rm TG}i_{\rm TG}$	1	JKT, Jan. 1991
Kar 203 B	V	1	
Kar 296 AB	$BVRI$	3	NOT, Jan. 1990
Arp 87	$BVRI$	3	Calar Alto, Feb. 1992
Kar 302 A	RI	4	Calar Alto, Feb. 1992
Kar 302 B	$BVRI$	3	
Kar 331 A	$BVr_{\rm TG}i_{\rm TG}$	2	NOT, July 1991
Kar 331 B	$BVr_{\rm TG}i_{\rm TG}$	2	
Arp 183	$BVr_{\rm TG}i_{\rm TG}$	2	NOT, Apr. 1993
Arp 36	$BVr_{\rm TG}i_{\rm TG}$	1	NOT, Apr. 1993
Kar 404 AB	$BVRI$	4	Calar Alto, Feb. 1992
NGC 5905	$BVRI$	3	Calar Alto, Aug. 1991
NGC 5908	$BVRI$	1	
Kar 471 A	$BVr_{\rm TG}i_{\rm TG}$	2	NOT, July 1991
Kar 471 B	$BVr_{\rm TG}i_{\rm TG}$	1	
Arp 218 AB	$BVr_{\rm TG}i_{\rm TG}$	2	NOT, Apr. 1993
Kar 523 A	$BVr_{\rm TG}i_{\rm TG}$	2	NOT, July 1991
Kar 523 B	$BVr_{\rm TG}i_{\rm TG}$	2	
Kar 538 A	B$i_{\rm TG}$	5	NOT, July 1991
Kar 538 B	B$i_{\rm TG}$	7	
Arp 298 AB	BVR	2	Calar Alto, Aug. 1991

After that the standard reduction steps followed. If the bias was structureless a constant value was subtracted, otherwise several bias frames were combined, smoothed and normalized to the overscan value, when available. Twilight flat-fields in each filter were taken each night except the 5$^{\rm th}$ night of the campaign in Calar Alto in 1991 and the 3$^{\rm th}$ night in 1992, in which cases the flat-fields of the previous nights were used. Several integrations in each field were co-added after the alignment to within a fraction of a pixel using the routines of IRAF. Cosmic rays and bad pixels and columns were eliminated by the procedures of IDL and IRAF. The R- and I-band images of Kar 296 and Arp 298 were saturated in a few nuclear pixels.

Since we are interested in surface photometry special attention was paid on correcting the sky gradients. In the final images the gradients were in most cases comparable to the sky background noise. In some images the global structure of the flat-field frames differed from that of the science frames and the strengths of the dust rings varied during some nights, probably because of the combined effects of dust in the chip and in the filterwheel: however their locations fortunately remained fixed and therefore could be mostly eliminated. When the galaxy was small compared to the total frame size, the median of the shifted science images was used as a correction frame.

The images of Calar Alto had a charge transfer problem: the signal levels of the images were dropped by 1−5 ADU's following bright point-like sources. This effect was corrected by adding a constant to the affected parts of the images. During the campaign of Jan. 1990 two gain factors were used. To obtain the same conversion of electrons to ADU's for the stars and galaxies, the star images were multiplied by a constant. The estimated error of the correction was 6%, based on measurements of one star, observed using both gain factors.

For flux calibration the lists of standart stars by Landolt (1983) and Landolt (1992) were used and 5−10 standard measurements per night in each filter were obtained. Bias, dark and flat-fied corrections for the standard stars were done and the instrumental magnitudes of one observing run were combined to fit the zero-points and color terms using the following equations:

$$
\begin{aligned}
b &= B + b_1 + b_2\,X + b_3(B-V)\\
v &= V + v_1 + v_2\,X + v_3(B-V)\\
v' &= V' + v'_1 + v'_2\,X + v'_3(V-R)\\
r &= R + r_1 + r_2\,X + r_3(R-I)\\
r' &= R' + r'_1 + r'_2\,X + r'_3(V-R)\\
i &= I + i_1 + i_2\,X + i_3(R-I),
\end{aligned}
$$

where b, v, r, and i are the instrumental magnitudes, B, V, V', R, R' and I the magnitudes in the Cousins system, b_1, v_1, v'_1, r_1, r'_1 and i_1 the zero-point coefficients, b_2, v_2, v'_2, r_2, r'_2 and i_2 the extinction coefficients, b_3, v_3, v'_3, r_3, r'_3 and i_3 the color terms and X is the air mass. Two alternative reductions for v and r are distinguished by primes. While the zero-points and color terms were calculated for each campaign, extinction was measured for each night. The color terms are small being only slightly larger than the error estimates of the

zero-point coefficients. The mean errors of the zero-points were 0.04 mag in B, V and I, and 0.03 mag in R.

Flux calibration for the campaigns at NOT prior to 1993 are complicated by the fact that the standard star magnitudes in the literature are in the Cousins photometric system, whereas we used Thuan-Gunn $r_{\rm TG}$ and $i_{\rm TG}$ filters. In that case transformations from Cousins to Thuan-Gunn system were applied for the Landolt standard stars using the transformation equations by Schombert et al. (1990):

$$r_{\rm TG} = R_{\rm c} + 0.280 + 0.038(R_{\rm c} - I_{\rm c}),$$

$$i_{\rm TG} = I_{\rm c} + 0.605 + 0.067(R_{\rm c} - I_{\rm c}).$$

For the observations of Arp 82 we had only one night in SPM so that it was not possible to do similar reduction as for the other galaxies. Instead, the flux calibration was performed by one standard star. Extinction was measured in B-band and approximated in the other bands by applying the average λ-extinction curve for SPM.

The total B-magnitudes and $B-V$, $V-R$ and $R-I$ color indices, measured by synthetic aperture photometry, are shown in Table 4, together with the B-magnitudes by de Vaucouleurs et al. (1991). Bright stars were eliminated and the few saturated pixels in the R- and I-images of Kar 296 and Arp 298 were replaced by the mean of the nearest pixels. The zero points of one of our campaigns (CA 1992) were shifted by 0.6 magnitudes in comparison with de Vaucouleurs et al., which has been taken into account in the magnitudes of Table 4. After this correction our measurements are in good agreement with the measurements by de Vaucouleurs et al.. The magnitudes are measured typically to the surface brightness of 26−27 mag/arcsec^2.

The color maps $B-V$, $B-R$, $V-R$, $B-I$, $V-I$ and $R-I$ were constructed by accepting only pixels above the 3σ level. The selection was made before converting the digital units to instrumental magnitudes and in construction of the color maps both images had to satisfy the criterion simultaneously in each pixel. In a few cases the sky gradient was larger than the 3σ level in which case the sky gradient was used as a selection limit for the accepted pixels. The images were rebinned (see Table 3) in order to reach a limiting surface brightness of about 27 mag arcsec^{-2}. The R-band image and the color maps $B-V$ and $R-I$ (if not otherwise mentioned) are shown in Fig. 2. A check of the reliability of our color images was made by comparing our $B-I$ map for NGC 5905 with the map by Wozniak et al. (1995): we measure the same mean $B-I=2.3$ along the dust lanes in the bar. Also the morphological characteristics of the two color maps are identical.

Table 4. Total magnitudes and color indices

Galaxy	B (*obs.*)	B (*lit.*[1])	$B-V$	$V-R$	$R-I$
Arp 70 A	14.77		0.95	0.61	0.38
Arp 70 B	16.13		0.99	0.51	0.54
Arp 74 A	14.76		0.96	0.57	0.55
Arp 74 B	17.40		1.24	0.56	0.52
Kar 64 A	13.58	13.42+0.13	0.47	0.14	0.26
Kar 64 B	14.92	15.08+0.13	0.68	0.20	0.34
Kar 125 A	12.90	12.7+0.30	0.77	0.59	0.45
Kar 125 B	13.77	13.8+0.30	0.89	0.73	0.32
Arp 82 A	13.30	13.19+0.18	0.68	0.51	0.65
Arp 82 B	14.81	14.75+0.18	0.62	0.44	0.60
Kar 168 A	12.60	12.74+0.18	0.64	0.76	0.12
Kar 168 B	15.16	15.40+0.20	0.30	0.49	0.16
Kar 179 A					
Kar 179 B	14.41	14.18+0.19	1.21	0.49	
Kar 203 A	13.83[2]			0.29	0.41
Kar 203 B	14.21[2]				
Kar 296 A	13.56	13.5+0.2	0.80	0.47	0.50
Kar 296 B	14.58	14.7+0.2	0.69	0.35	0.41
Arp 87 A	13.86		0.53	0.45	0.17
Arp 87 B	15.23		0.42	0.74	0.03
Kar 302 A	10.49[3]				0.35
Kar 302 B	13.24		0.55	0.04	0.50
Kar 331 A	13.53	13.66+0.18	0.81	0.53	0.73
Kar 331 B	15.42		0.94	0.40	1.15
Arp 183	14.61	14.4+0.2	0.44	0.54	0.86
Arp 36	15.42		0.40	0.20	1.04
Kar 404 A	12.54	12.65+0.13	0.56	0.75	0.60
Kar 404 B	13.84	13.62+0.18	0.50	0.69	0.49
NGC 5905	12.59	12.59+0.17	0.77	0.42	0.69
NGC 5908	12.96	13.01+0.13	0.86	1.34	0.22
Kar 471 A	13.88	13.90+0.18	0.57	0.06	0.48
Kar 471 B	14.35	14.27+0.19	0.64	0.40	0.41
Arp 218 A	15.28	15.35+0.18	0.52	0.53	0.15
Arp 218 B	16.80		0.81	0.54	0.38
Kar 523 B	14.08	13.74+0.18	0.46	0.59	0.54
Kar 523 A	15.65		0.73	0.85	0.76
Kar 538 A	14.04	13.80+0.19	1.60[4]		
Kar 538 B	14.94	14.90+0.20	1.68[4]		
Arp 298 A	12.94	13.0+0.11	0.57	0.59	
Arp 298 B	14.97	15.08+0.12	0.66	0.87	

[1] From The Third Reference Catalogue of Bright Galaxies (de Vaucouleurs et al. 1991).
[2] V-magnitude.
[3] R-magnitude.
[4] $B-I$.

4. Discussion of the main characteristics of the galaxies

We consider as M51-type the following pairs: Arp 36, Arp 70, Arp 74, Arp 82, Arp 86, Arp 87, Arp 183, Arp 218, Kar 64, Kar 168, Kar 296, Kar 302 and Kar 404. It is worth noticing that not only large galaxies, like Arp 86, but also rather small ones like Kar 302 can have well developed, strong spiral arms. Arp 298 is considered marginal, because the spiral arms are not as strong and deeply penetrating as for the other members of this category, being more ring-like. The main galaxy is classified as a Seyfert 1. It has a nuclear ring in $B-V$, as found earlier in optical broad band images by Buta & Crocker (1993). This is an interesting characteristic because, contrary to Seyfert 2 galaxies, Seyfert 1 nuclei are not generally found to have extended nuclear starbursts. Although the redshifts of the companions are not known for Arp 70, Arp 74 and Arp 36, and for neither of the components of Arp 218, interpreting them as interacting pairs is clear on morphological bases. However, for Arp 183, which also lack redshift measurement the interaction is less clear, since the presumed companion is over 4 magnitudes fainter. Incidentally, Arp 36 resides at a distance of 8 galaxy diameters from Arp 183 and has approximately the same recession velocity, but for its large separation most probably does not have any significant current influence on Arp 183.

Altogether, 8 out of 13 M51-type pairs with sufficient information (excluding Arp 298), have blue $B-V$ colors in the central regions of the companions (Arp 82, Arp 86, Kar 64, Kar 168, Arp 87, Kar 302, Arp 36, and Kar 404) and only one of them in the main galaxy (Arp 74). The large number of active companions is quite suprising because gas content of normal galaxies is not able to sustain long-lived starburst activity. For example, in NGC 7752, the companion of Arp 86, a starburst of the present strength would consume all gas of its disk in about 200 Myr (Laurikainen et al. 1993). However, if there is mass transfer from the main galaxy to the companion, this may have triggered a nuclear starburst or extended star formation in the central regions of the companion, and provide the required source of gas. In some of the companion galaxies, like in Arp 87 or Arp 82, the blue central regions are partly obscured either by dust or the red stellar component. Three of the above pairs (Arp 82, Arp 87 and Kar 302) show knotty star forming regions in the tail-arm opposite to the companion and one of them (Kar 296) in the bridge arm (see the $R-I$ maps). Arp 87 is listed as a possible candidate for polar-ring galaxies by Whitemore et al. (1990). It is also worth noticing that the companion in Kar 404 has extremely blue spiral arms.

The pairs that do not have blue $B-V$ colors in the central regions of the companions are Arp 70, Arp 183, Arp 218, Arp 74 and Kar 296. However, Arp 70 has small nuclear $R-I$ color, which hints to recent star formation: the small $R-I$ value is supposed to be due to strong Hα and NII emission lines, emanating through the continuum. This rises the number of companions with enhanced star formation to 9. For Kar 296 one of the inner spiral arms of the companion has blue $B-V$ color. Except for Kar 296, the above pairs show more dispersed spiral structures than the M51-type pairs of our sample in general. Additionally, Arp 70 and Arp 218 have warps thus indicating that the companions may not be orbiting in the plane of the main galactic disk.

Arp 36 is classified as an M51-type system by Vorontsov-Velyaminov (1977) and is suggested to show a bar and a double companion at the end of the single developed arm. We also consider Arp 36 as M51-type system, but for a different reason: which to Vorontsov-Velyaminov is a bar, appears to us a system of two galactic nuclei, both connected to their own spirals, and a strong HII-region. Due to their $R-I$ colors the knots at the end of the well developed arms are most probably strong HII-regions, not galaxies as suggested by Vorontsov-Velyaminov. The smaller galaxy in the system (about $10''$ N−W) has blue nuclear $B-V$ color. This is an interesting system, because it may represent an example of M51-type pairs in a late phase of evolution. Similarly, Arp 183 has very dispersed spiral arms.

The remaining non M51-type pairs show large-scale instabilities some of them manifesting as strong color gradients in their disks. The main characteristics for some individual pairs are listed below:

Kar 203 and Kar 125 are spiral-spiral pairs with galaxy separations of 1−1.5 main galaxy diameters. All four galaxies show morphological peculiarities and the spiral arms are rather dispersed and irregular. At least one galaxy in both pairs shows strong $B-V$ color gradient throughout the disk (Kar 203 B and Kar 125 A; for Kar 203 A we do not have color maps). The $R-I$ images have no noticable gradients, but instead show knotty star forming regions in the same galaxies.

Kar 471 B, like Kar 203 B and Kar 125 A, has a $B-V$ gradient and knotty star forming regions. However, in this case the color gradient is rather a color difference between the two arms rather than a gradient through the disk. The companion, Kar 471 A, has strong one-sided star forming region in the inner disk (see the $R-I$ image).

Kar 523 is a pair of two barred galaxies. Kar 523 B has a dust lane on the right side between the outer arm and part of the inner pseudoring. There is also star formation along the bar and in a small region in the nucleus, detected in $B-V$. In the $R-I$ image one can also see a nuclear ring, about $5''$ in diameter, but it might be an artefact caused by seeing. However, rebinning the images by a factor of 4 left the ring still visible.

NGC 5905/5908. NGC 5905 is a barred galaxy with a nuclear ring, about $5''$ in diameter, detected in $B-V$, found earlier by Wozniak et al. (1995).

Kar 331 is an exception in our sample because both galaxies are lenses, otherwise it looks like an M51-type

pair. Kar 331 A has a nuclear ring visible in $B-V$, about $10''$ in diameter, and the isophotes of the galaxy are twisted. The bright nearby object in the images of Kar 331 A is a star.

Acknowledgements. E. Laurikainen and H. Salo wish to thank Instituto de Astronomia UNAM (Mexico) for its hospitality during their visit, when part of the reductions were carried out. Special thank to Irene Cruz-González, Margarita Rosado, Deborah Dultzin and Etienne Le Coarer for their interest to this project which led to collaboration in Fabry-Perot and IR-observations. We also thank Prof. G. Paturel for his most valuable comments.

References

Arp H., 1966, Atlas of Peculiar Galaxies, ApJS 14, 1
Bergvall N., Laurikainen E., Johansson L., Aalto S., 1997, manuscript
Buta R., Crocker D.A., 1993, AJ 105, 1344
de Vaucouleurs G., de Vaucouleurs A., Corwin H.G., et al., 1991, The Third Reference Catalogue of Bright Galaxies. Springer-Verlag, New York
Karachentsev I., 1972, Catalogue of Isolated Pairs of Galaxies in the Northern Hemisphere, Soobsch S.A.O. 7, 3
Landolt A.U., 1983, AJ 88, 439
Landolt A.U., 1992, AJ 104, 340
Laurikainen E., Salo H., 1997, (Paper II) (in preparation)
Laurikainen E., Salo H., Aparicio A., 1993, ApJ 410, 574
Paturel G., Fouqué P., Bottinelli L., Gouguenheim L., 1989, Catalogue of Principal Galaxies, observatoire de Lyon, France, (PGC)
Salo H., Laurikainen E., 1993, ApJ 410, 586
Salo H., Laurikainen E., 1997a (submitted)
Salo H., Laurikainen E., 1997b (submitted)
Schombert J.M., Wallin J.F., Struck-Marcell C., 1990, AJ 99, 497
Telles E., Terlevich R., 1995, MNRAS 275, 1
Vorontsov-Velyaminov B.A., 1977, A&A 28, 1
Whitmore B.C., Lucas R.A., McElroy D.B., Steinman-Cameron T.Y., Sackett P.D., Olling R.P., 1990, AJ 100, 1489
Wozniak H., Friedli D., Martinet L., Martin P., Bratschi P., 1995, A&AS 111, 115
Zaritsky D., Rix H.-W., Rieke M., 1993, Nat 364, 313

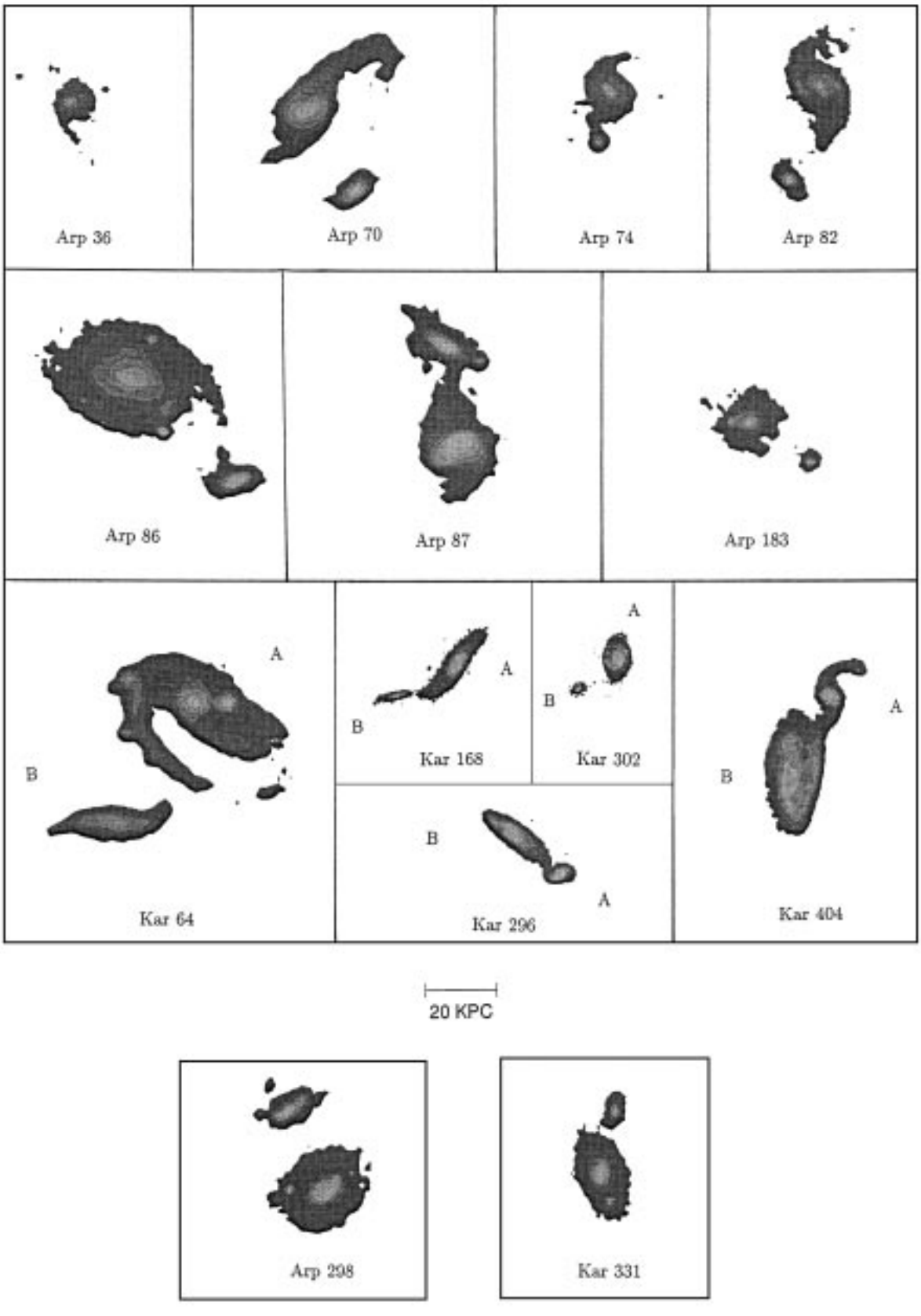

Fig. 1. Digital Sky Survey images for the sample pairs. All galaxies are displayed in the same linear kpc-scale, the distance estimated from the recession velocity of the primary galaxy with $H_0 = 75$ km s^{-1} Mpc^{-1}. **a)** shows the M51-type pairs (and two marginal cases: Arp 298 and Kar 331), and **b)** the other pairs. Arp 218 is not displayed since there are no redshift measurements

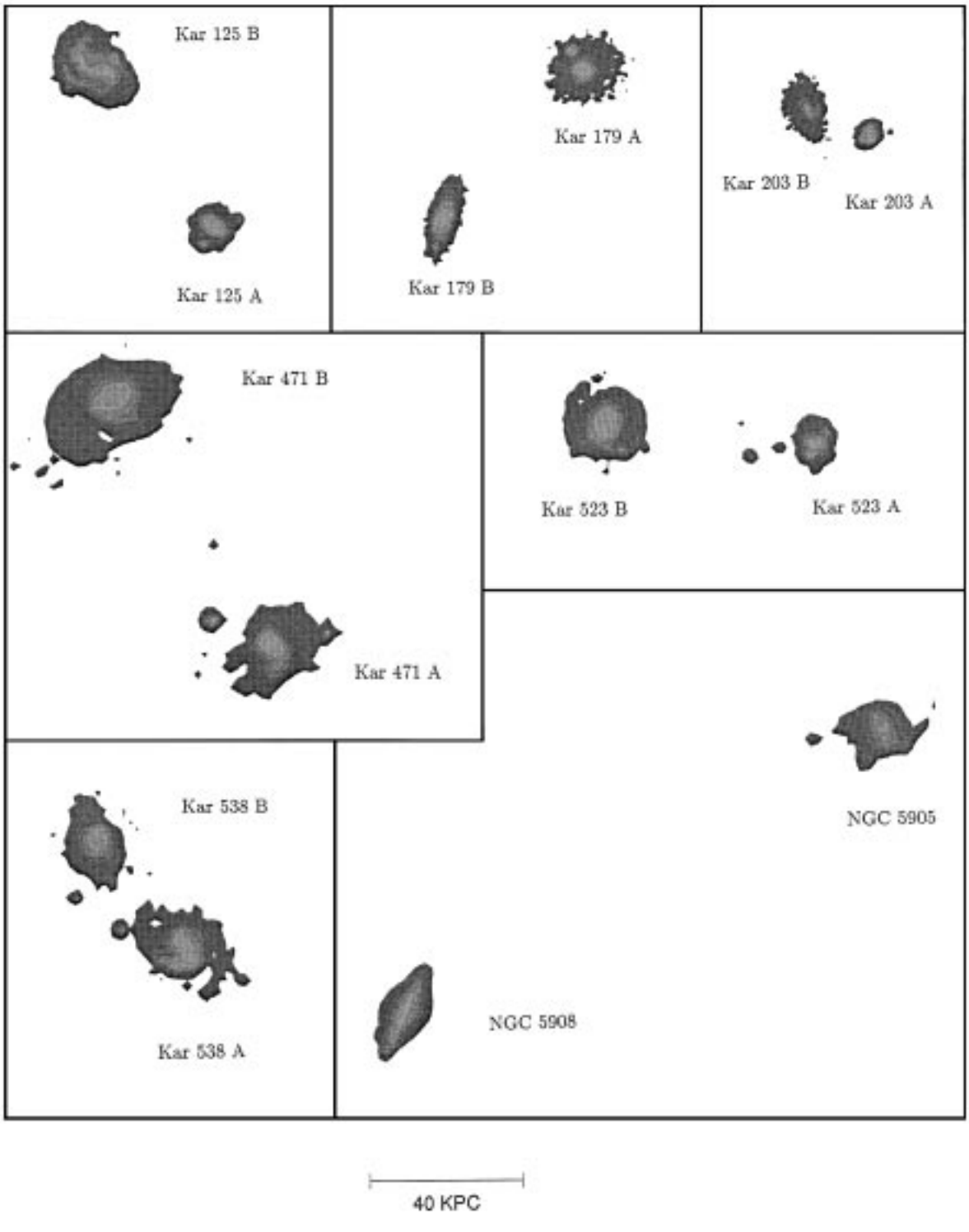

Fig. 1. continued

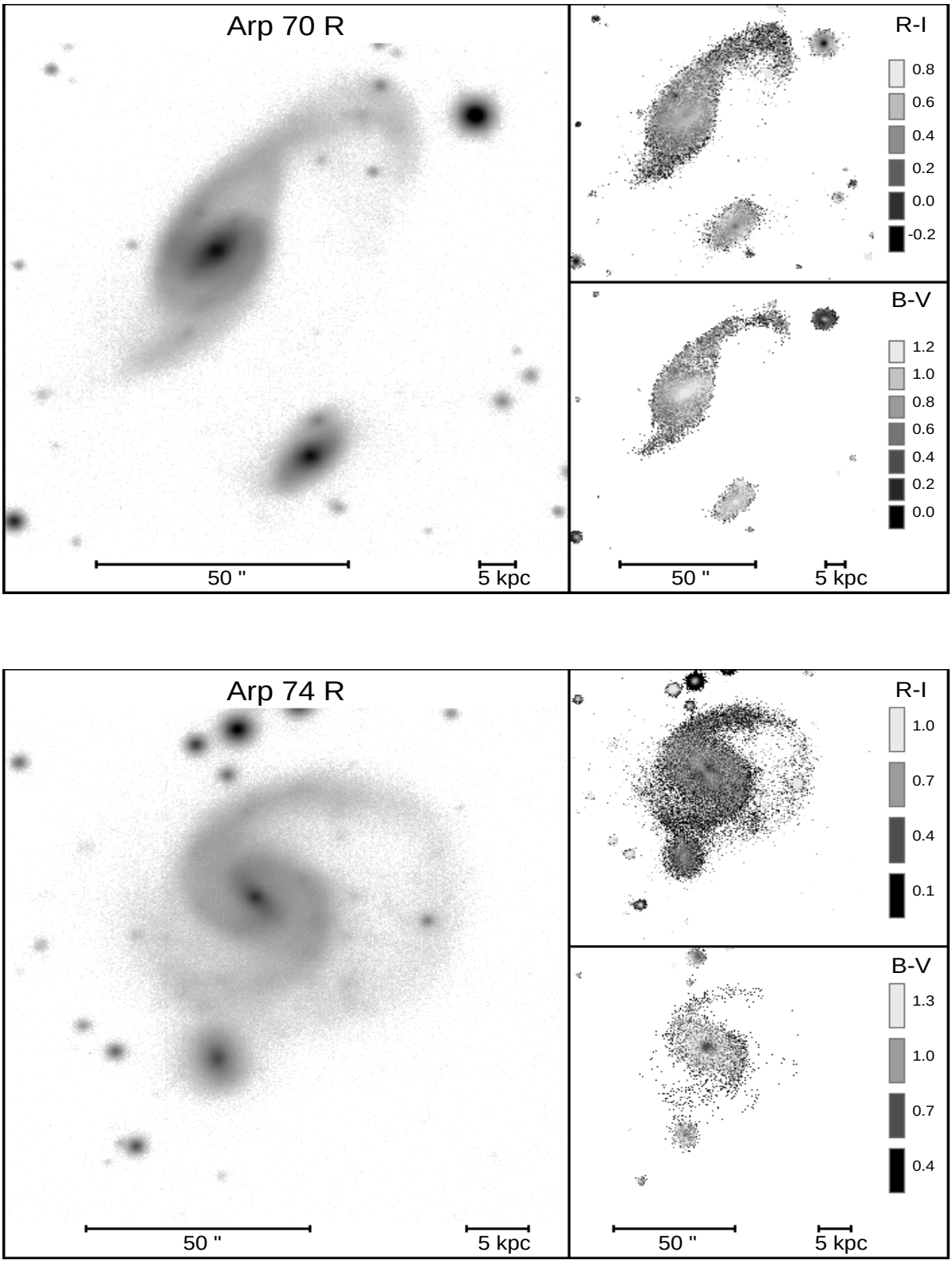

Fig. 2. Direct R-band image and the color indice maps $R-I$ and $B-V$ (if not otherwise indicated in the figure). The R-band frame is the cleaned image displayed in a logaritmic scale. The color indice maps are constructed from rebinned images, accepting only pixels above the 3σ level: the rebinning yields a limiting surface brightness of 27 mag/arcsec^2. In all images North is up and Est is left. Vertical bars denote the angular scale and the absolute linear scale, calculated as in Fig. 1

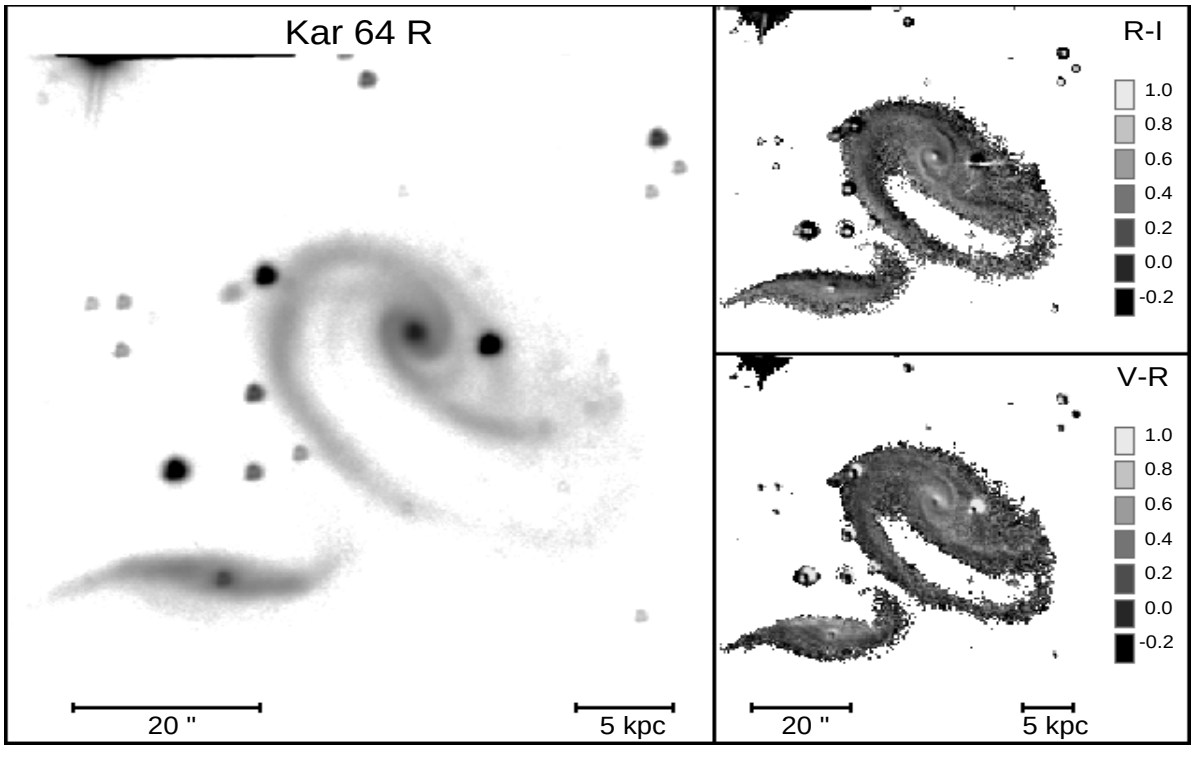

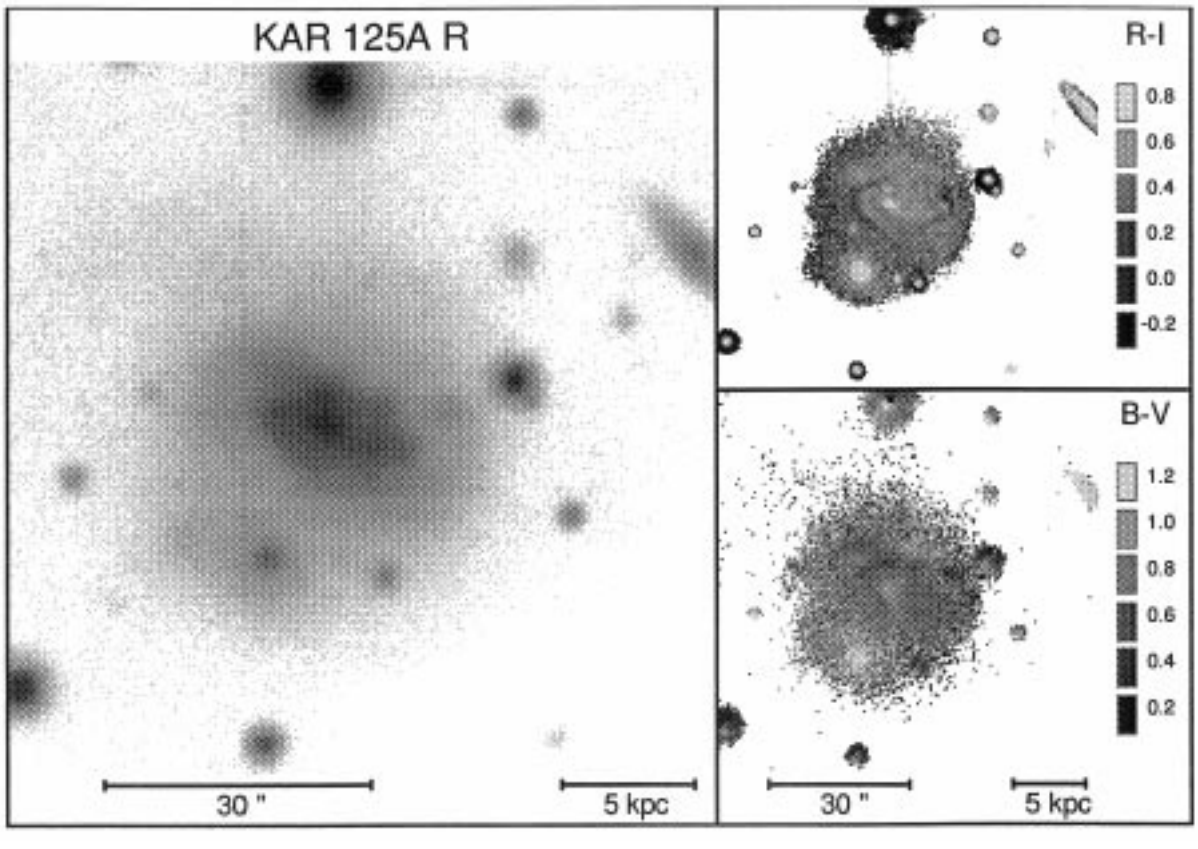

Fig. 2. continued

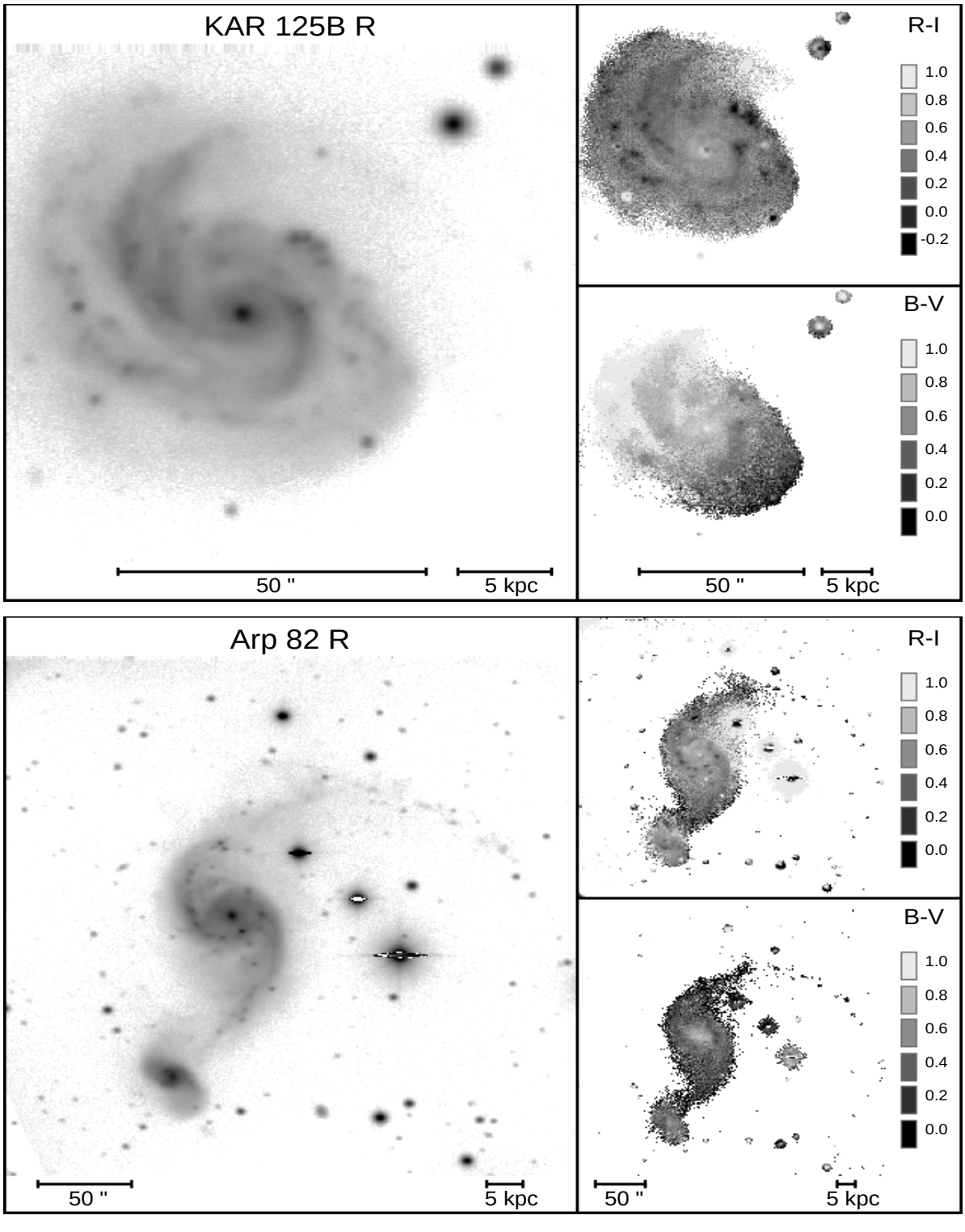

Fig. 2. continued

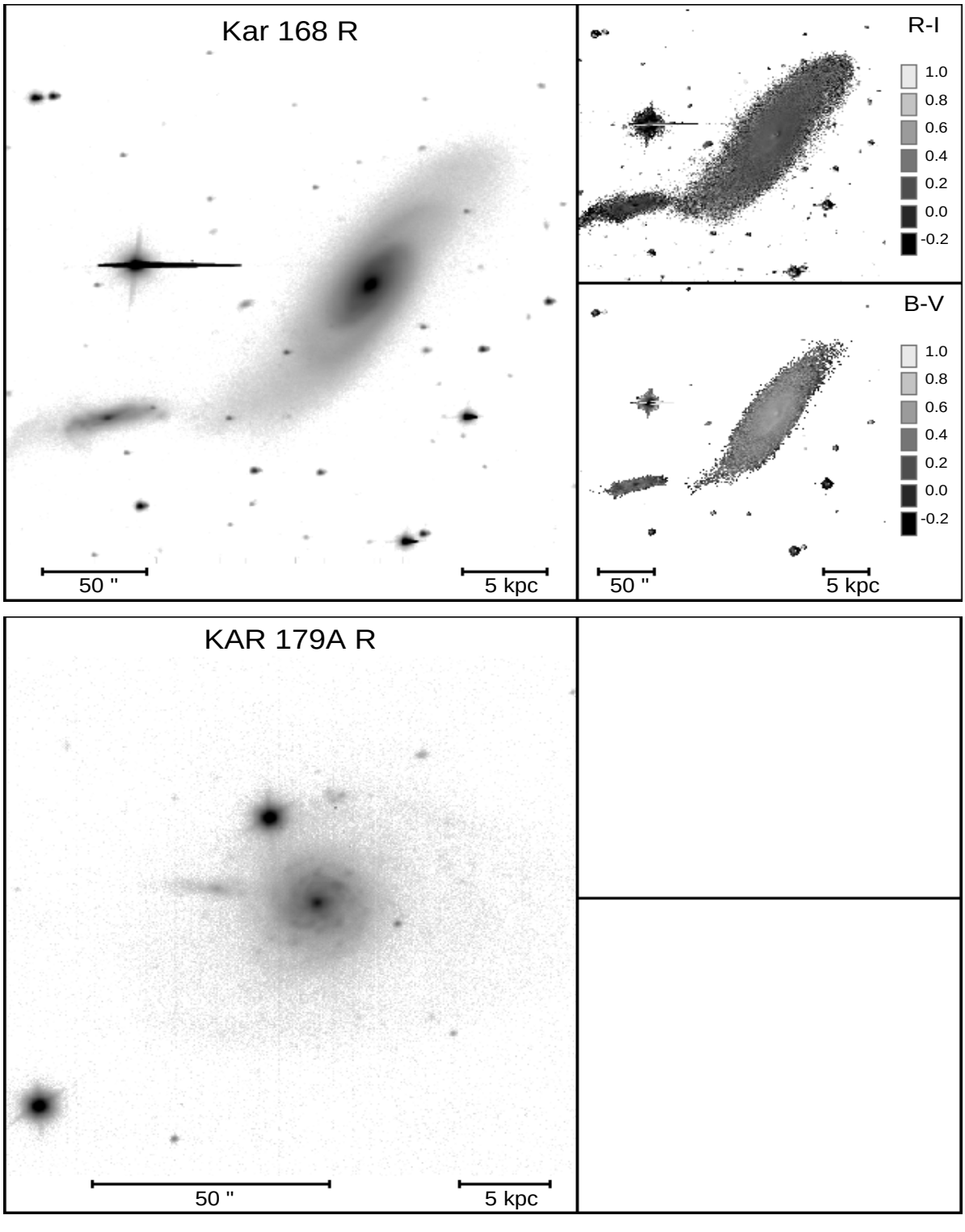

Fig. 2. continued

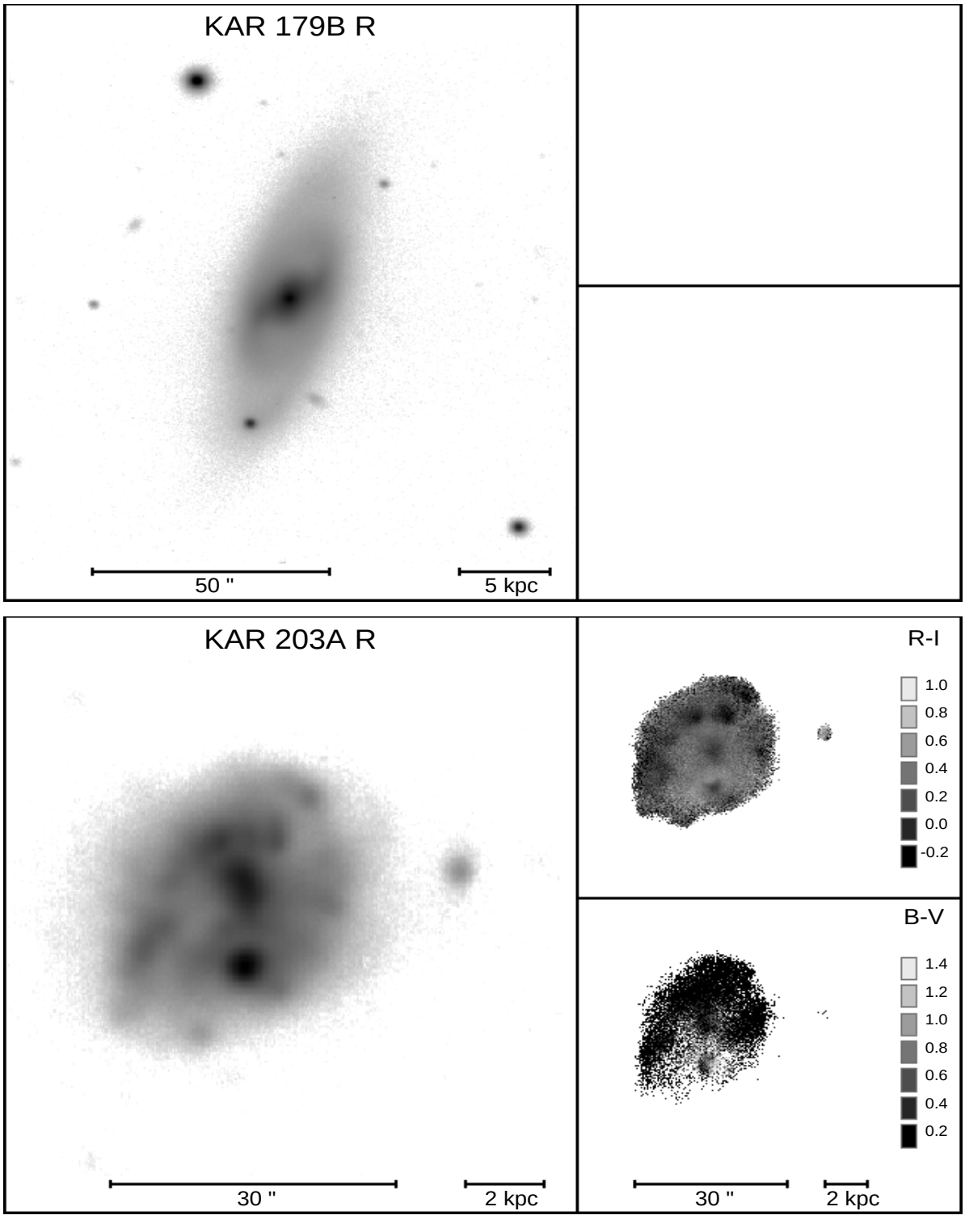

Fig. 2. continued

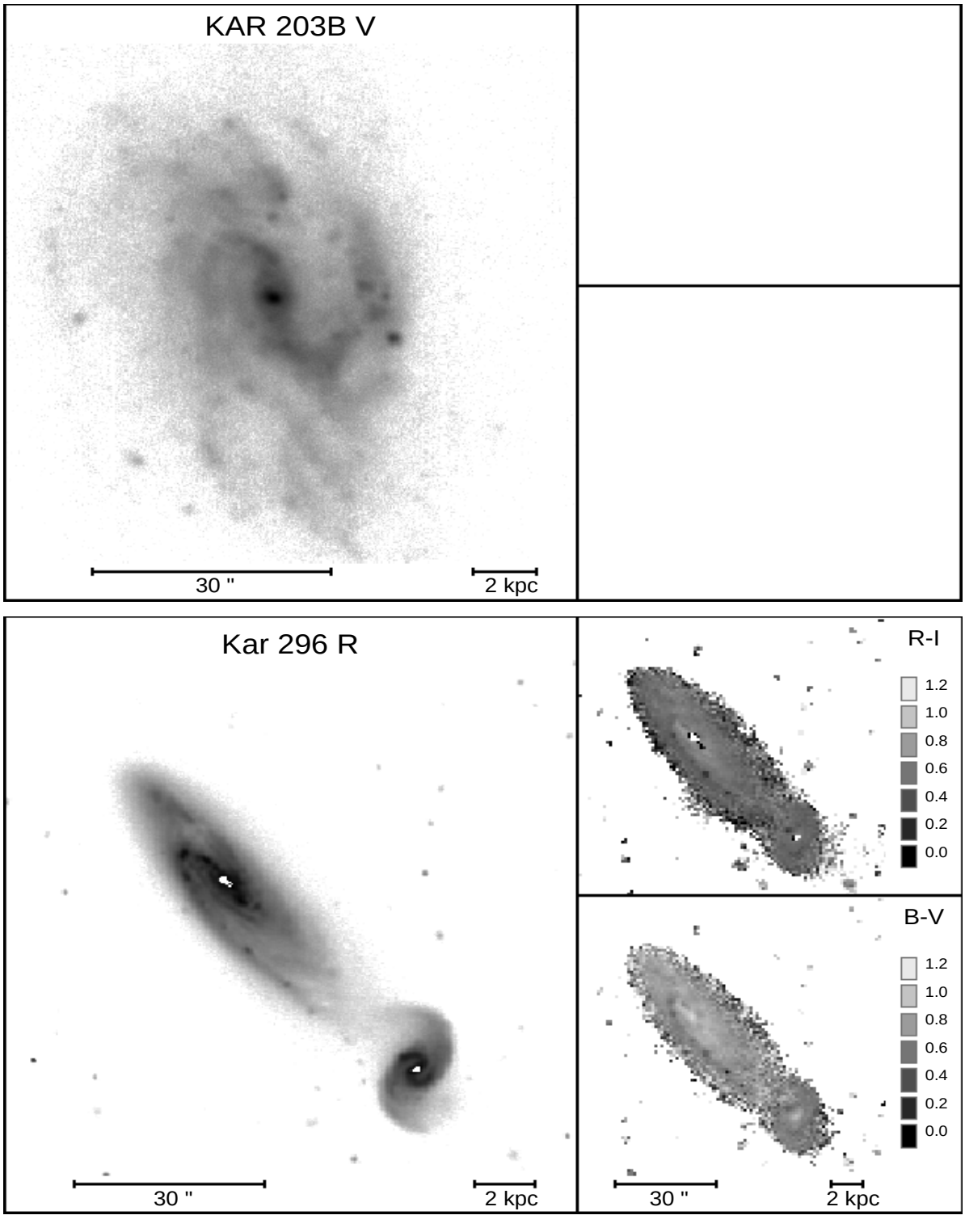

Fig. 2. continued

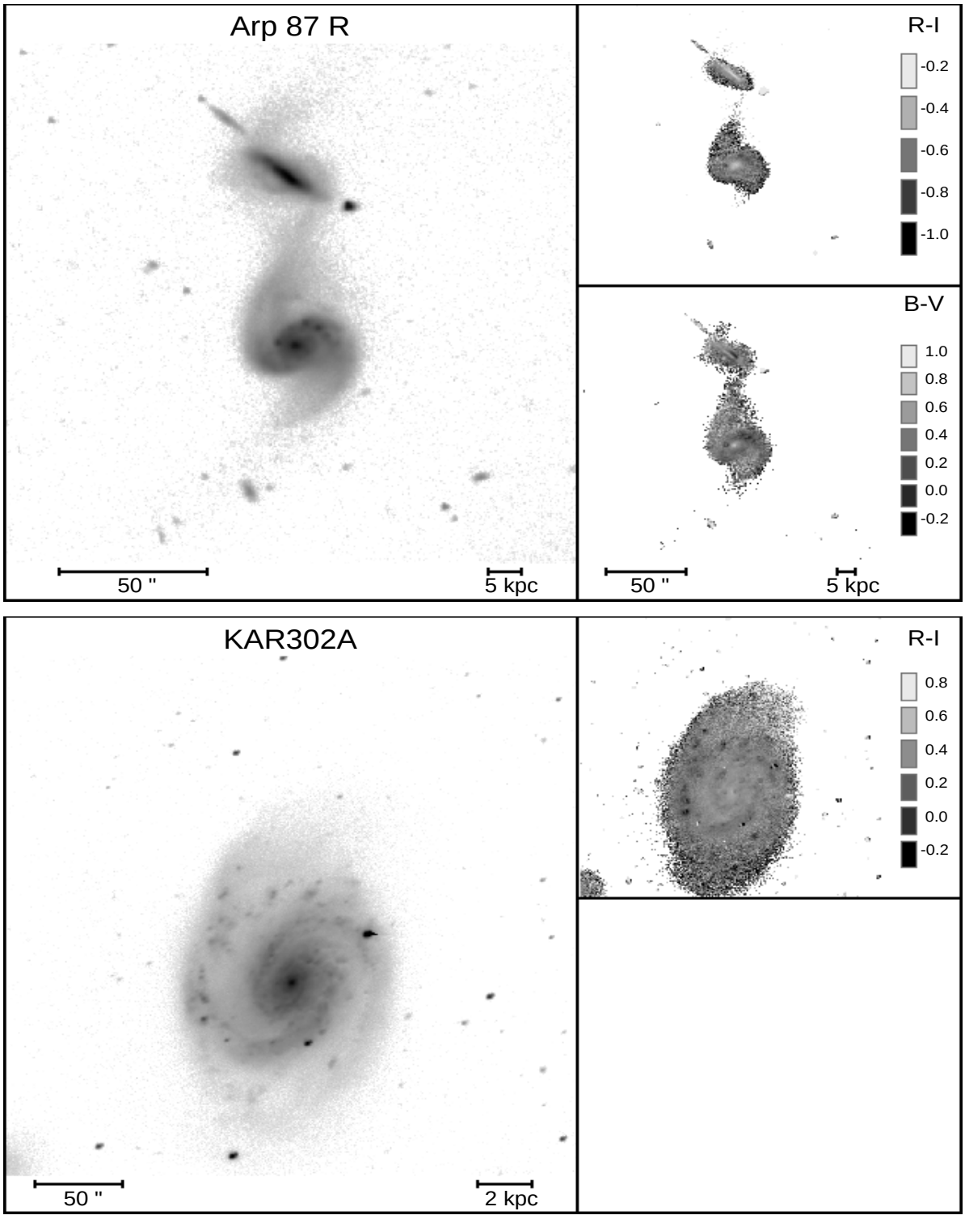

Fig. 2. continued

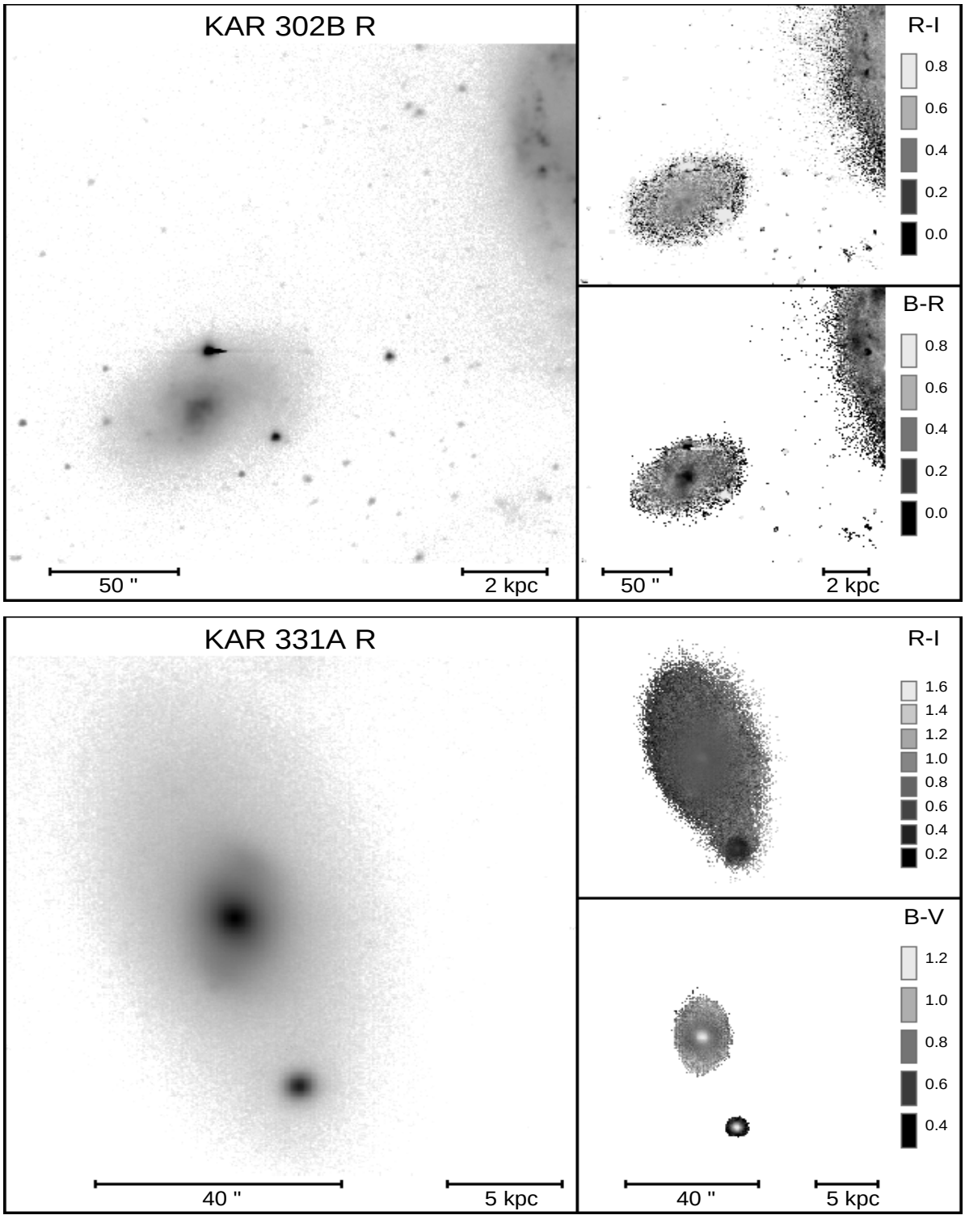

Fig. 2. continued

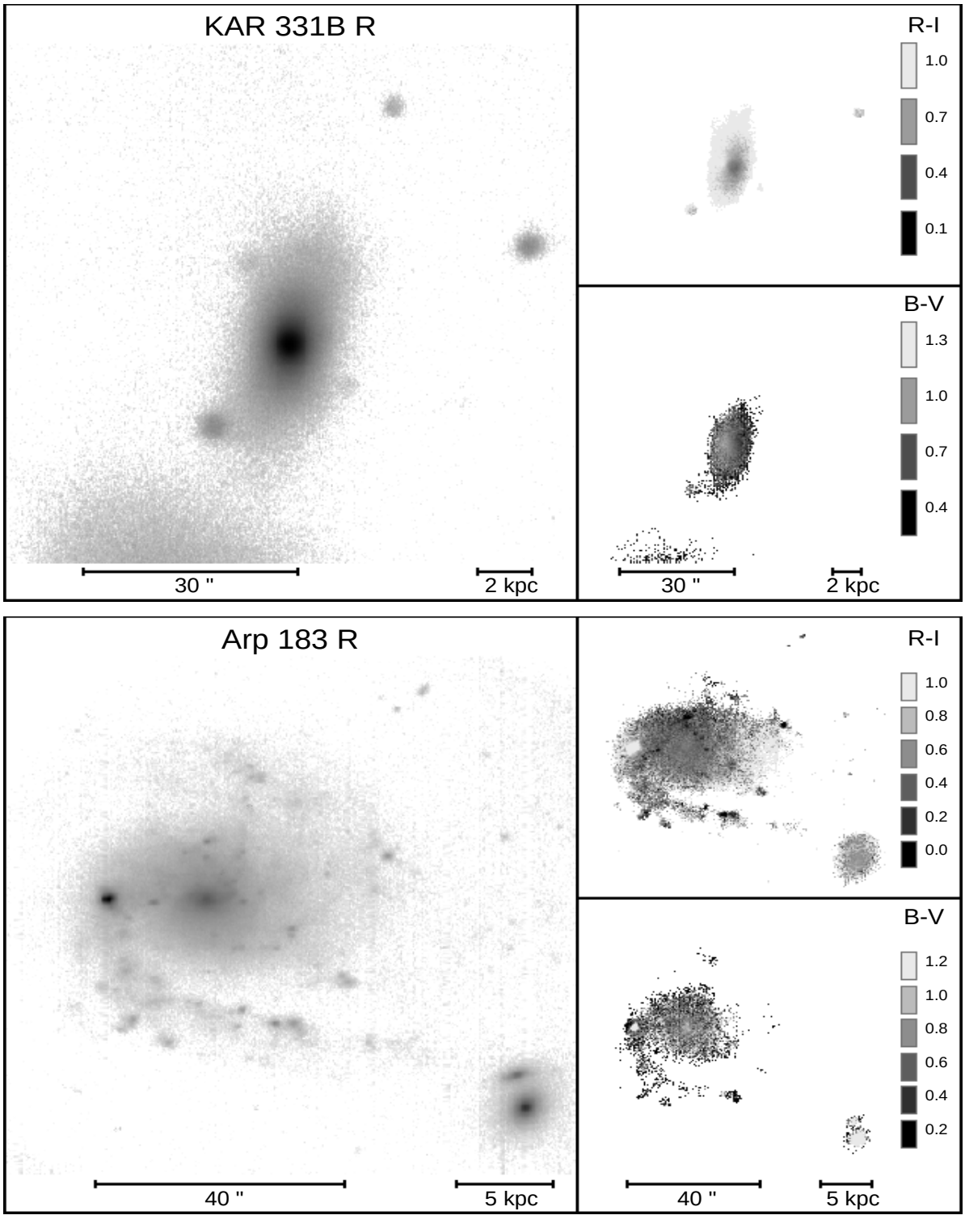

Fig. 2. continued

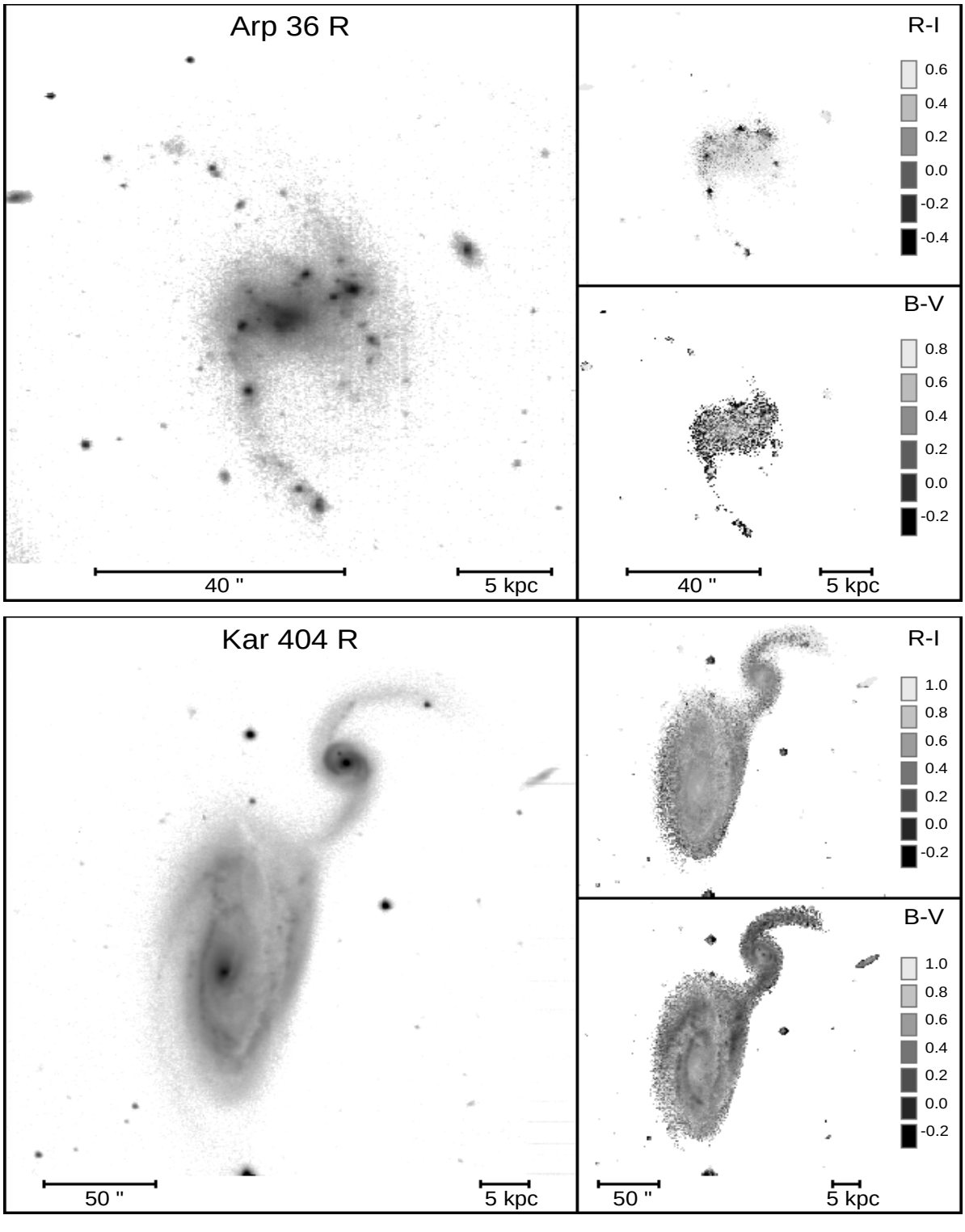

Fig. 2. continued

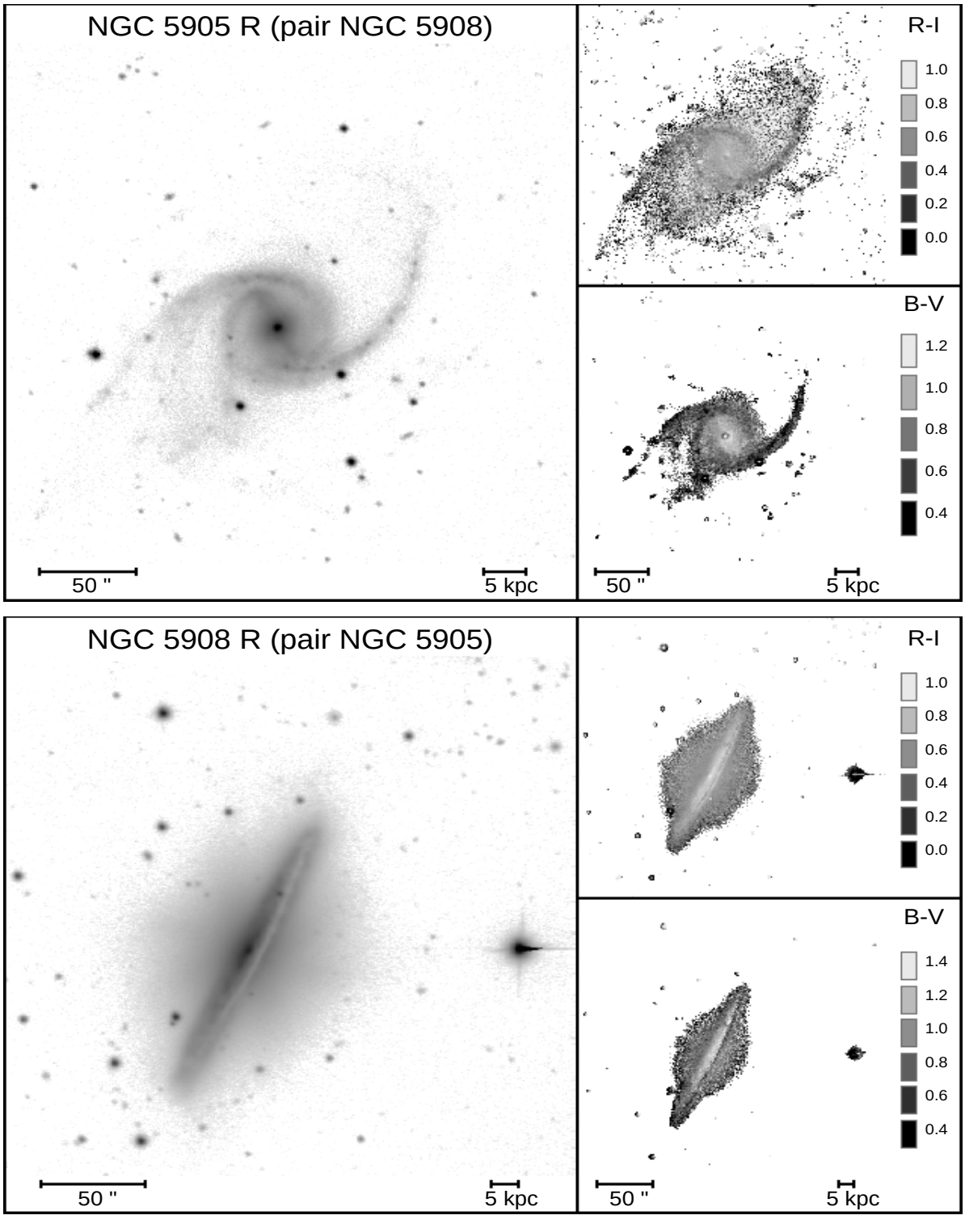

Fig. 2. continued

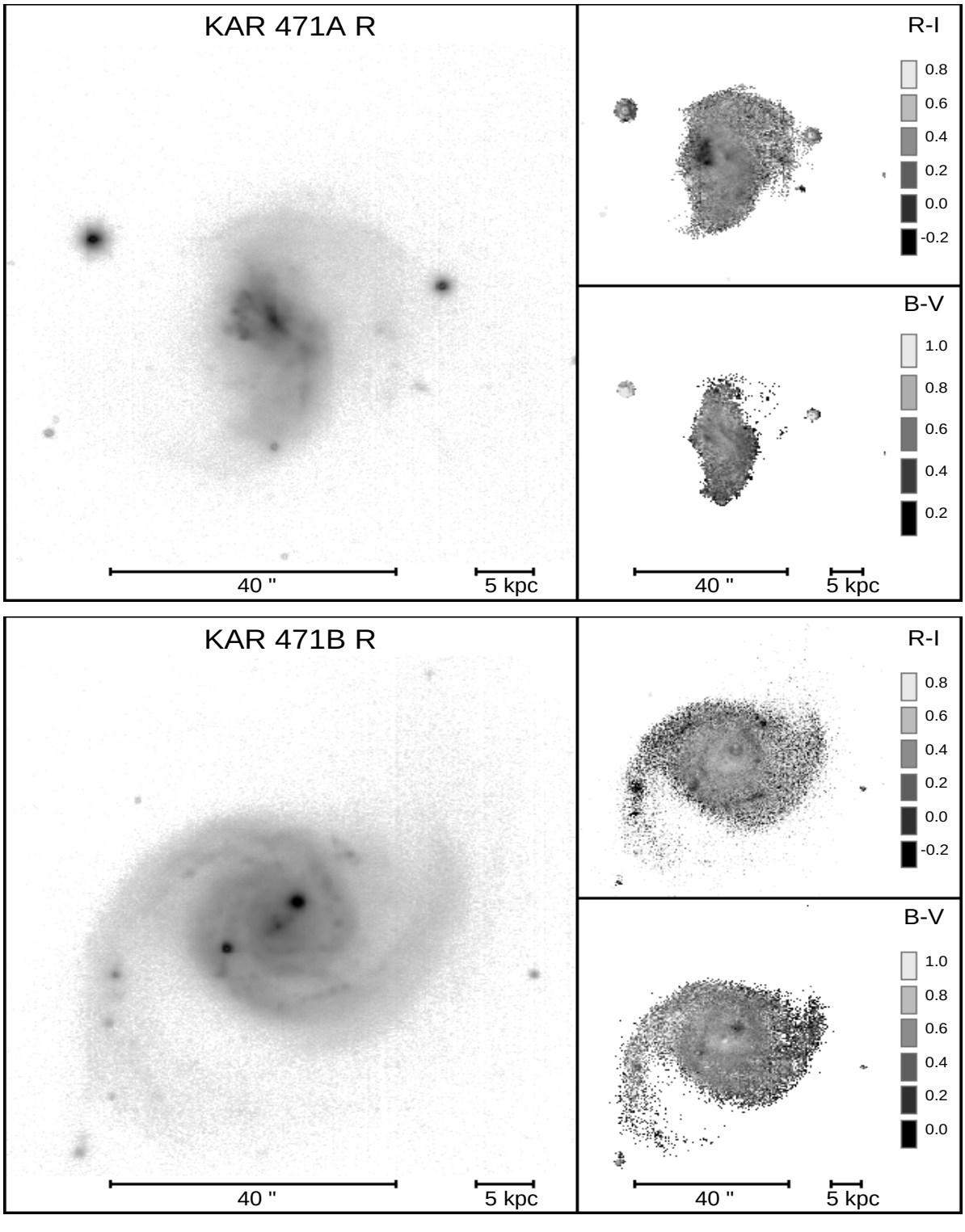

Fig. 2. continued

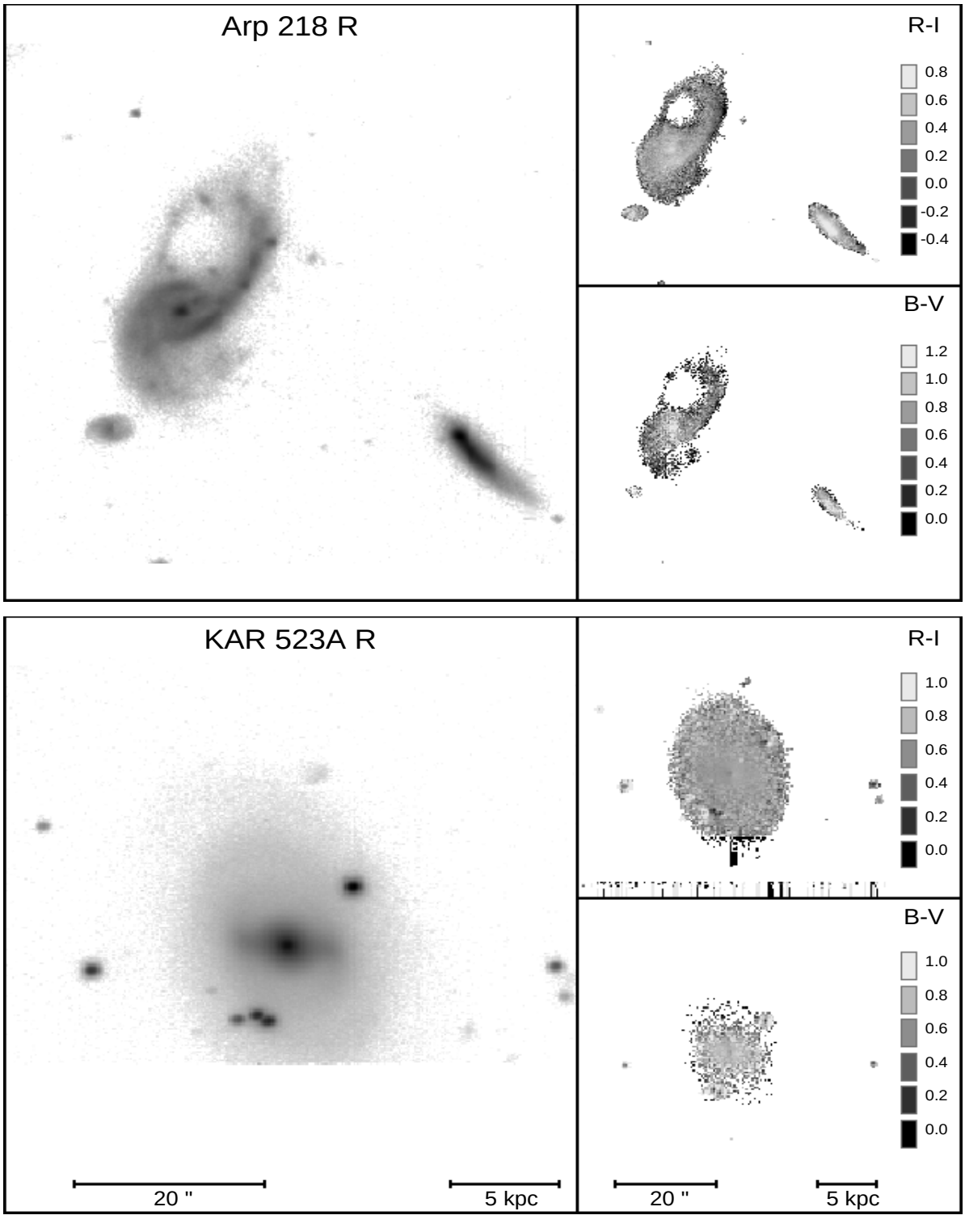

Fig. 2. continued

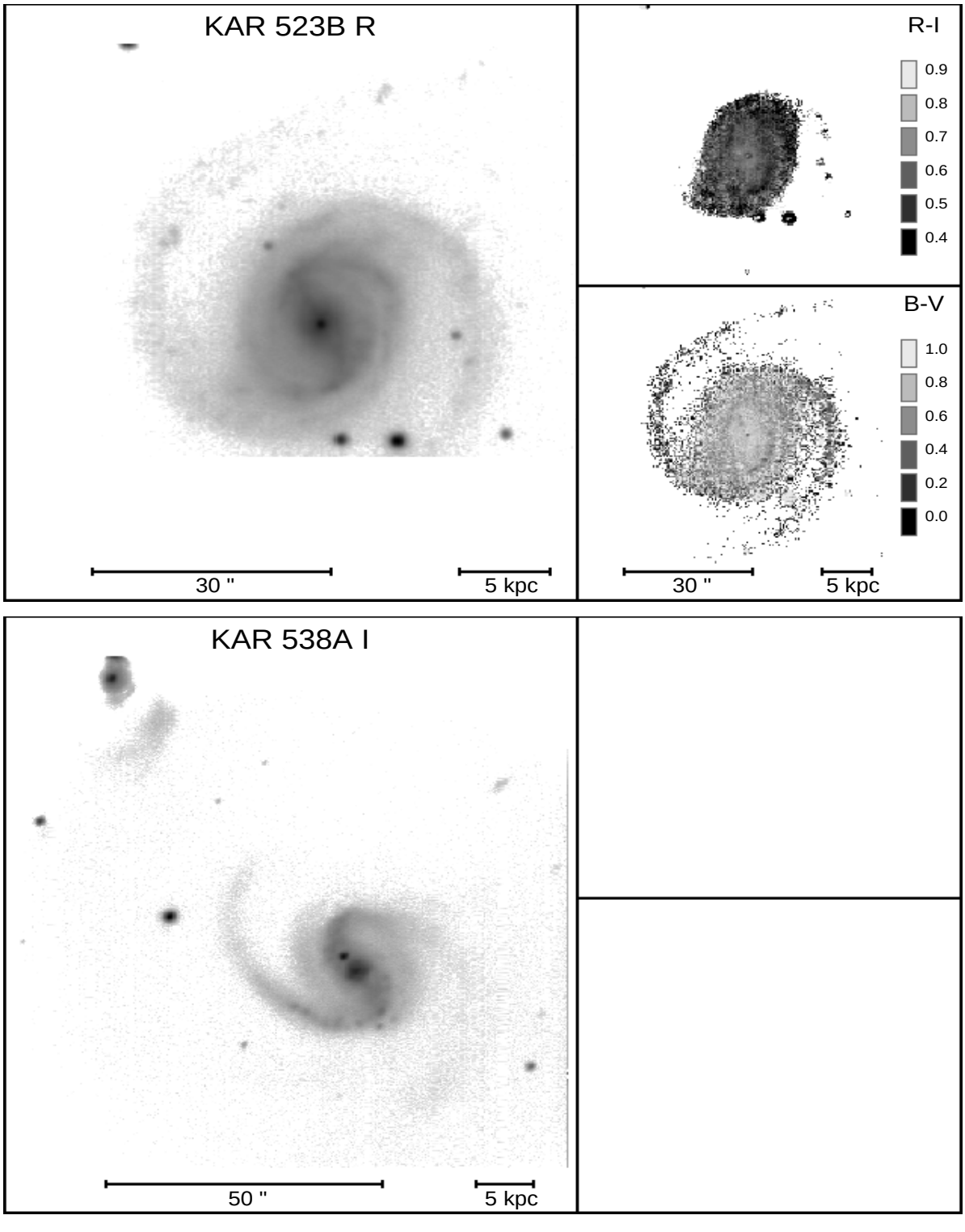

Fig. 2. continued

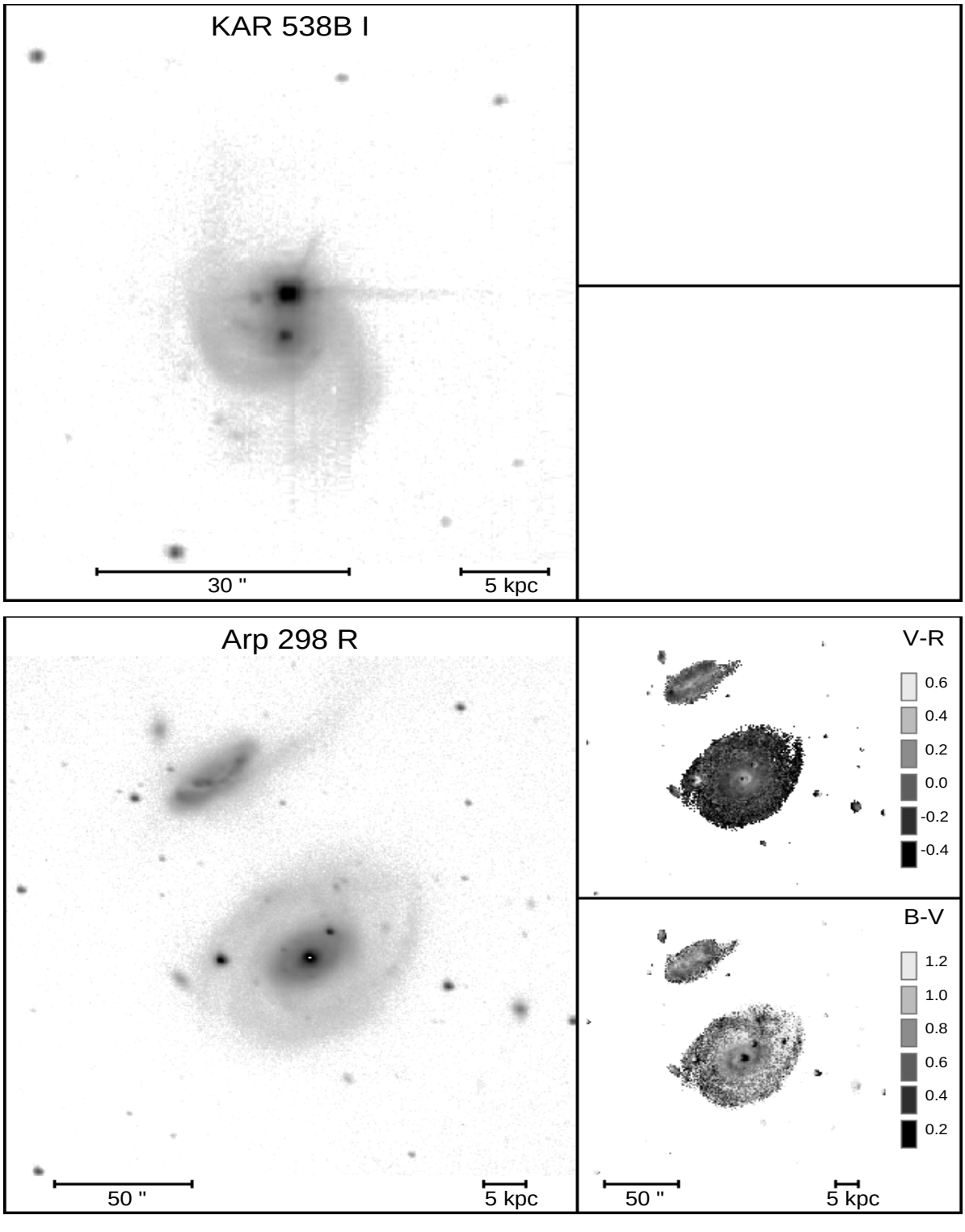

Fig. 2. continued